IL NUOVO CIMENTO **39 C** (2016) 283
DOI 10.1393/ncc/i2016-16283-0

COMMUNICATIONS: SIF Congress 2015

Morphological studies of gamma-ray sources with IACT arrays

L. AMBROGI

Gran Sasso Science Institute - viale Francesco Crispi 7, 67100 L'Aquila (AQ), Italy

received 5 February 2016

Summary. — The potential of a next-generation ground-based gamma-ray telescope to perform morphological studies of celestial gamma-ray sources is investigated. With this aim, general analytical expressions for the instrument response are derived and simulations of isolated source are used as a benchmark to understand the telescope performance. The morphology is represented assuming an ideal Gaussian point spread function (PSF) and a non-Gaussian PSF with extended tails. The response of the telescope is also tested in case of complex environments. In particular, the effect of locating the source (i) nearby a second one and (ii) on top of a diffuse halo-type object is investigated. The first scenario is particularly interesting in the framework of Galactic objects, where the presence of more than one single source in the same field of view (FoV) is expected. The latter represents a relevant study in the contest of extended extra-galactic sources surrounding AGNs.

1. – Introduction

Cosmic gamma-rays are abundantly produced in many Galactic and Extragalactic sources and they freely propagate in space without deflection by interstellar and intergalactic magnetic fields. These two peculiar characteristics make these high-energy photons perfect astrophysical messengers, carrying information about non thermal processes in the Universe. Moreover, at very high energies, gamma-rays can be effectively detected by ground-based instruments and, among different techniques, the Imaging Atmospheric Cherenkov Telescope (IACT) technique has proven to be the most promising approach. The great potential of IACT observatories has been demonstrated by the current generation of ground-based gamma-ray telescopes. The spectral and morphological studies above few tens of GeV performed in the recent years by HESS [1], MAGIC [2] and VERITAS [3], led to impressive results in the astroparticle field, proving the potentiality and feasibility of this detection technique as a truly observational discipline, especially when operated with the stereoscopic approach. Thanks to these excellent scientific results, the currently operating telescopes paved the way to the next generation IACT array. Indeed, in few years from now, the Cherenkov Telescope Array (CTA) observatory will be fully operational and will represent the most advanced future project in the field. CTA is

expected to cover a wide energy range, exploiting an excellent angular and energy resolution and a huge detection area which should guarantee a factor 10 improved sensitivity in comparison to the existing gamma-ray instruments. In this work the CTA observatory has been used as a template for the description of a generic next-generation IACT array observing the sky with tens of telescopes and the performance of this instrument has been studied [4].

2. – Instrument response

A CTA-like instrument has been defined making use of the publicly available Monte Carlo (MC) calculations performed by the CTA Consortium for a possible layout of the southern array [5](1). In particular, in the energy range from 50 GeV to 100 TeV an analytical parametrization for the effective area, the background rate and the angular resolution has been found. As shown in ref. [6] (fig. 3), for the layout of CTA South observatory considered, and assuming $z = \log(E/1\,\mathrm{TeV})$, the effective detection area A_{eff} can be parametrized with the following expression:

$$A_{\mathrm{eff}}(z) = \frac{A}{1 + B \cdot \exp\left(-\frac{z}{C}\right)}, \tag{1}$$

where the saturation value of the effective area is $A = 4.36 \cdot 10^6\,\mathrm{m}^2$, while $B = 6.05$ and $C = 3.99 \cdot 10^{-1}$ define the rate of change of A_{eff} with respect to the energy. The background rate, after the rejection cuts, has been estimated by the CTA Consortium through detailed simulations of cosmic rays (CR) interacting in the atmosphere, including the noise from the night-sky background (NSB) and the electronic one [7]. The energy dependence of the background rate per square degree can be approximated as

$$\mathrm{BgRate}(z) = A_1 \cdot \exp\left(-\frac{(z-\mu_1)^2}{2\sigma_1^2}\right) + A_2 \cdot \exp\left(-\frac{(z-\mu_2)^2}{2\sigma_2^2}\right) + C, \tag{2}$$

with $A_1 = 3.87 \cdot 10^{-1}\,\mathrm{Hz/deg}^2$, $\mu_1 = -1.25$, $\sigma_1 = 2.26 \cdot 10^{-1}$, $A_2 = 27.4\,\mathrm{Hz/deg}^2$, $\mu_2 = -3.90$, $\sigma_2 = 9.98 \cdot 10^{-1}$ and $C = 3.78 \cdot 10^{-6}\,\mathrm{Hz/deg}^2$, as presented in ref. [6] (fig. 5). The energy-dependent angular resolution can be described in the form

$$\sigma_{\mathrm{PSF}}(z) = A \cdot \left[1 + \exp\left(-\frac{z}{B}\right)\right], \tag{3}$$

with $A = 2.71 \cdot 10^{-2}\,\mathrm{deg}$ representing the best angular resolution achievable with the telescope layout considered in this work and $B = 7.90 \cdot 10^{-1}$ the scaling factor which tells how fast the angular resolution changes with energy. For the corresponding distribution, see fig. 1 in ref. [6]. The angular resolution used here is defined as the 68% containment radius of the PSF. For what concern the PSF shape, the standard assumption is to treat it as a Gaussian

$$f_{\mathrm{PSF}} = \exp\left(\frac{x^2 + y^2}{2\sigma_{\mathrm{PSF}}^2}\right), \tag{4}$$

(1) The CTA performance file can be accessed at:
`https://portal.cta-observatory.org/Pages/CTA-Performance.aspx`

with $\sigma_{\rm PSF}$ being the value of the angular resolution. Nevertheless, tails extending far away form the Gaussian peak might be present and modify the actual shape of the PSF, as already observed in a wide variety of instruments working in different intervals of the electromagnetic spectrum. In order to take into account also this realistic scenario, a non-Gaussian PSF with tails has been defined. Following ref. [8], a representation of the non-Gaussian PSF has been given in the form

$$f_{\rm PSF} = \exp\left(\frac{x^2+y^2}{2\sigma^2_{\rm PSF}}\right) + K \cdot \exp\left(\frac{x^2+y^2}{2\sigma^2_{\rm PSFtails}}\right), \tag{5}$$

where the parameter $\sigma_{\rm PSFtails}$ has been fixed to the value 0.2 deg, while different hypotheses on the ratio K of the two Gaussians have been considered: 0.3, 0.1, 0.5, 0.01 and 0.001. The higher the contribution of the tails, *i.e.* the larger the parameter K, the stronger the modification of the PSF shape with respect to the ideal Gaussian case.

3. – Morphological studies of isolated sources

The presence of the tails in the PSF can compromise proper morphological studies due to their additional fake emission which might be erroneously reconstructed as a typical feature of the source morphology. Simulations of excess maps of isolated sources have been performed assuming both the Gaussian and the non-Gaussian PSF (eqs. (4) and (5), respectively), and used as a benchmark to test and understand the instrument response. The background events have been uniformly distributed in the map according to the predictions described by eq. (2), whereas the gamma-ray source has been simulated assuming a Gaussian spatial distribution characterized by the source angular size $\sigma_{\rm src}$ and centered on the point $(X_0, Y_0) = (0, 0)$ deg

$$f(x,y) = S \cdot \exp\left(-\left(\frac{(x-X_0)^2}{2\sigma^2_{src}}\right) + \left(\frac{(y-Y_0)^2}{2\sigma^2_{src}}\right)\right). \tag{6}$$

The factor S in eq. (6) takes into account the strength of the gamma-ray source, for which a Crab-like power-law spectrum in the form

$$\mathrm{d}N/\mathrm{d}E = n \cdot N_0 \times (E/1\,\mathrm{TeV})^{-\Gamma} \tag{7}$$

has been considered, with $\Gamma = 2.62$ as measured in ref. [9]. The flux strength is given in units of Crab flux at 1 TeV: $N_0 = 2.83 \cdot 10^{-11}\,\mathrm{TeV}^{-1}\,\mathrm{cm}^{-2}\,\mathrm{s}^{-1}$. For the reconstruction of source morphology, the Gaussian shape of the source (eq. (6)) has been convolved with the ideal PSF, described also by a Gaussian function (eq. (4))

$$f(x,y) = S \cdot \exp\left(-\left(\frac{(x-X_0)^2}{2(\sigma^2_{src}+\sigma^2_{\rm PSF})}\right) + \left(\frac{(y-Y_0)^2}{2(\sigma^2_{src}+\sigma^2_{\rm PSF})}\right)\right). \tag{8}$$

Equation (8) has been used to fit the skymaps not only in the case of the Gaussian PSF, but also when applying the PSF tails in the source simulation. The assumed ignorance on the actual shape of the PSF, avoiding any correction due to the non-Gaussian modeling of the PSF at the fitting and reconstruction level, allows us to study possible misinterpretations of the results due to the presence of the tails.

Using a sample of tens of simulation realizations and considering $\sigma_{\rm PSF}$ as a fixed parameter, the morphological parameters of the source have been estimated through a χ^2-fitting analysis. In particular, in order to understand the effect of the presence of the tails in the PSF, the angular size of an isolated source with $\sigma_{\rm src} = 0.1\,{\rm deg}$ has been reconstructed assuming a non-Gaussian PSF. Note that when the modeling of the PSF is described by eq. (5), the case $K = 0.001$, *i.e.* negligible tails contribution, can be considered as a rough approximation of the ideal Gaussian PSF [6].

In the low-energy domain, *i.e.* from 50 to 100 GeV, the background dominates over the signal and the reconstruction of the source parameters is affected by fluctuations for flux strengths lower than ∼0.1 Crab, as shown in ref. [6] (fig. 10). For brighter sources, a proper estimation of the size of the source can be done when the ratio K is in the range of 0.001–0.01. At these energies, the similar value of the angular resolution ($\sigma_{\rm PSF} \sim 0.15\,{\rm deg}$) and of the size of the tails ($\sigma_{\rm PSFtails} = 0.2\,{\rm deg}$), results in a relatively low effect of the tails for small values of K. Nevertheless, when K is large enough ($K \geq 0.05$), the PSF is affected and so is the estimation of the source size. For the very high energies, *i.e.* $E \geq 10\,{\rm TeV}$, the effect of the tails is more evident due to the better value of the angular resolution ($\sigma_{\rm PSF} \sim 0.03\,{\rm deg}$) with respect to $\sigma_{\rm PSFtails}$, which critically modifies the final shape of the PSF. Depending on the actual value of K, the reconstructed size turns out to be overestimated: the larger the value of K, the more significant the deviation from the expected value, to the point where the reconstruction saturates at the size of the tails, *i.e.* 0.2 deg. In case of large photon statistics combined with a very good instrument sensitivity, $\sigma_{\rm PSFtails}$ represents the minimum size one can aim to reconstruct, since even a weak emission artificially induced by the tails of the PSF can be detected by the telescope.

4. – Morphological studies of multiple sources

The capability to reconstruct the source morphology might be compromised in case of crowded fields, where a complex distribution of the sources might limit the instrument performance. Two different scenarios are studied in this section: (i) the case of two nearby objects, which represent a key issue when planning observation of the Galactic plane region and (ii) the case of a compact source on top of a diffuse halo-type emission, which might be relevant in the framework of extended extra-Galactic sources surrounding AGNs.

4˙1. *Two nearby Gaussian sources.* – The case of two nearby sources has been simulated for different separation distances between the two objects. As for the isolated objects, the CR background has been uniformly distributed in the map and a Gaussian spatial distribution (eq. (6)) has been used for the gamma-ray sources. The centers of gravity of the two sources have been estimated through a χ^2-fitting analysis and from the reconstructed positions the distance between the two sources has been calculated. In fig. 1 the reconstructed distances between the two sources is shown for different combinations of their flux strengths, while their spectra are described by eq. (7). The true distance, $d_{\rm true}$, is shown for each plot, ranging from 0.2 deg to 0.5 deg, and a Gaussian PSF is assumed. Obviously, the larger the distance the better the reconstruction. For small separation between the sources, the distance is well estimated only when the flux levels of the two sources are similar. Otherwise the reconstruction fails, leading to a null separation, since the weakest source turns out to be hidden by the companion and only the strongest of the two objects is visible. These plots are referred to the CTA core

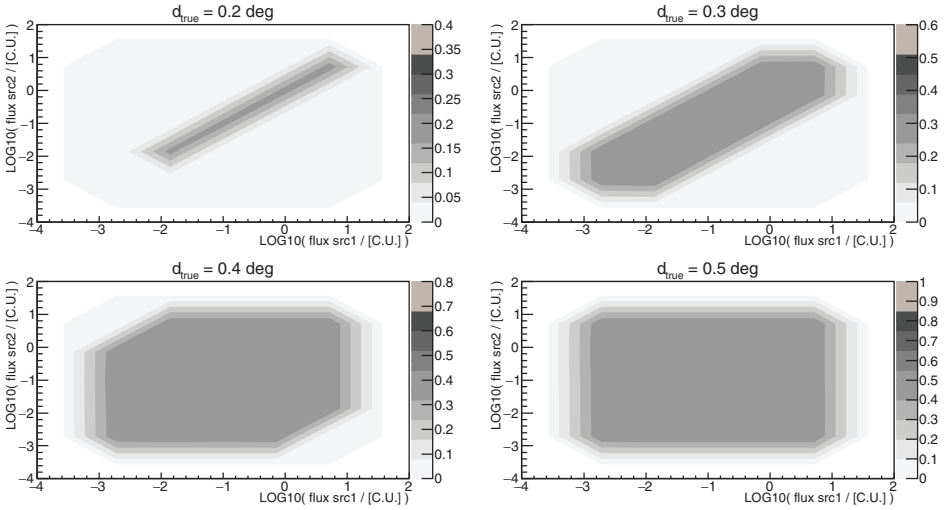

Fig. 1. – Reconstructed distance in 50 hours observation between two Gaussian sources (named *src*1 and *src*2 in the plots) for different combinations of the flux strengths of the two objects. The true distances used in the simulation, d_{true}, are shown on the top of each distribution, ranging from 0.2 deg to 0.5 deg. The energy interval is from 1 TeV to 10 TeV and the Gaussian PSF is assumed (eq. (4)).

energies, from 1 TeV to 10 TeV, where the best sensitivity of the instrument is expected to be achieved [5]. When the lowest energies are considered, the effect of a larger σ_{PSF}, which for E $\in$ [0.05–0.1] TeV is as large as $\sim$0.15 deg, affects the capability to isolate the two objects since it strongly correlates the events in the map. This effect adds to a larger background rate and to the *hiding-effect*, resulting in the inability to individually distinguish the two sources.

These studies have been repeated also under the assumption of a non-Gaussian PSF. Equation (5) has been calculated for $K = 0.3$ which represents the worst scenario in terms of effects induced by the presence of the tails in the PSF. The fake emission from the tails adds to the gamma emission of the sources. For separations in the range of those shown in fig. 1, the distance is always estimated as zero, since the presence of the tails does not allow to resolve the two sources anymore. The effect of the tails disappears only when the distance between the two sources is large enough (d $\geq$ 0.7 deg). In fig. 2 the reconstructed distance between the two sources, placed at distances ranging from 0.7 deg to 1.4 deg, is shown. To disentangle two point-like sources a minimum distance of $\sim$0.8 deg is required.

4˙2. *A compact Gaussian source on a diffuse, halo-type, extended source.* – The problem of separating from each other two different sources also occurs when observing a very bright central source surrounded by a diffuse halo. Simulations of this scenario have been performed, assuming a Gaussian spatial distribution for the central source (eq. (6)) and exploiting the following function to describe the extended halo:

$$f(x,y) = Z \cdot \frac{1}{2} \cdot \left(\tanh\left(\frac{r + R_{\mathrm{halo}}}{\delta} \right) - \tanh\left(\frac{r - R_{\mathrm{halo}}}{\delta} \right) \right), \tag{9}$$

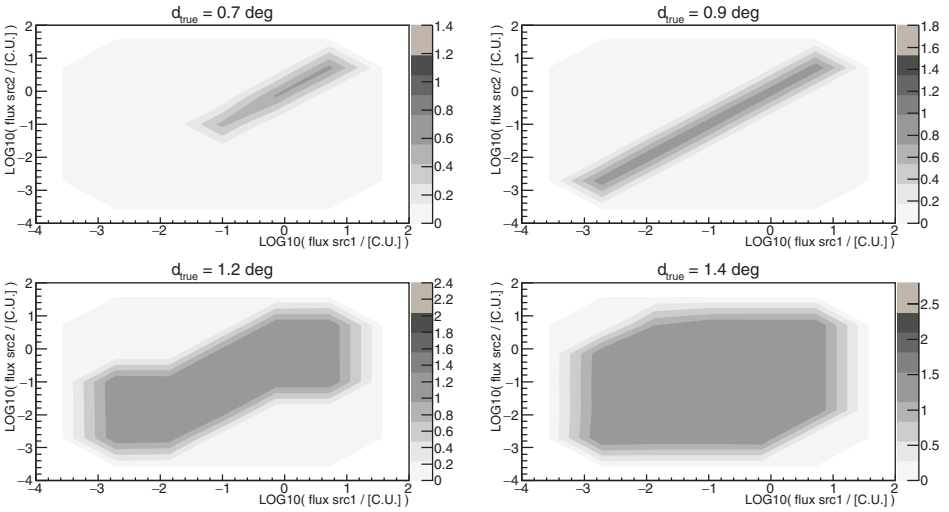

Fig. 2. – Same as in fig. 1 but for the case of a non-Gaussian PSF with tails, calculated for $K = 0.3$ (eq. (5)). The true distances used in the simulation, ranging from 0.7 deg to 1.4 deg, are shown on the top of each distribution.

with $r = \sqrt{(x - X_0)^2 + (y - Y_0)^2}$. This hyperbolic tangent function is a smooth approximation of a 2D circular Heaviside function and δ is a parameter that roughly controls the thickness of smooth transition zone; here $\delta \to 0$ is assumed. The halo has been centered at $(X_0, Y_0) = (0, 0)$ deg and its radius has been defined as: $R_{\rm halo} = \sigma_{\rm src} + m \cdot \sigma_{\rm PSF}$, with $m = [1, 2, 5, 10, 30]$. The factor Z in eq. (9) defines the intensity of the halo flux, expressed in units of the flux strength of the central source, *i.e.* $Z = k \cdot (\mathrm{d}N/\mathrm{d}E)_{\rm CentralSrc}$ with $k = [0.001, 0.01, 0.1, 1, 10, 100]$. Also in this case, the spectrum defined by eq. (7) is used for the two objects.

The two sources are efficiently separated when both the halo and the central source are individually well reconstructed. In fig. 3 the reconstructed angular size of the central source (on the left) and the reconstructed radius of the halo (on the right) are shown as a function of the halo flux strength and keeping the flux of the central source fixed at 0.1 Crab. The Gaussian PSF is assumed and the energy range from 1 to 10 TeV is considered, where the average value of the angular resolution is $\sigma_{\rm PSF} = 0.042$ deg. When the flux level of the halo is small enough, *i.e.* $\leq 10\%$ of the central source flux, the reconstruction of the angular size of the compact object is well performed, since the weak emission from the halo doesn't compromise the observation of the central source. On the other hand, when the two fluxes start to be of the same magnitude, the reconstructed $\sigma_{\rm src}$ deviates from the expected value: for $R_{\rm halo} \gtrsim 2\sigma_{\rm src}$ the extended emission from the halo adds to the emission due the central source which, in turn, results to be overestimated ([2]). Otherwise, when the halo emission is limited in space ($R_{\rm halo} \lesssim 2\sigma_{\rm src}$), the reconstructed source size is underestimated, due to the high photon density induced by the halo emission in the region of the compact object. Inversely, for what concerns the reconstruction of

([2]) Note that the central object is defined by eq. (6) and therefore the 95% of its spatial distribution is comprised in 2 standard deviations from the peak value, *i.e.* $2\sigma_{\rm src}$.

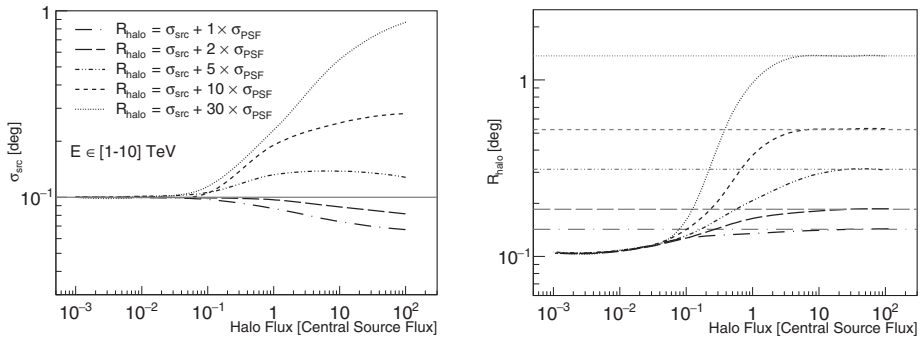

Fig. 3. – Left: reconstructed angular size of the central source as a function of the halo flux, which is expressed as a fraction of the compact object flux and kept at 0.1 Crab. The solid line is for the real value of the source size, *i.e.* $\sigma_{\rm src} = 0.1\,$deg. Different curves are for different values of the halo radius. Right: reconstructed radius of the halo as a function of the halo flux. The horizontal lines indicate the expected values; different line styles are for the different input radius used in the simulation and listed in the legend on the left. The energy range considered here is from 1 to 10 TeV where $\sigma_{\rm PSF} = 0.042\,$deg and the best sensitivity of the instrument is expected. The observation time is 50 hours and the Gaussian PSF is assumed (eq. (4)).

the halo radius, the estimation of $R_{\rm halo}$ saturates to a threshold value roughly given by $\sigma_{\rm src}$ in case of a faint halo emission. In this configuration, the strong emission from the central object at 0.1 Crab prevents the isolation of the diffuse halo and makes the reconstruction of the halo morphology unreliable. The only possibility to extract the halo from the central source is to deal with a bright and extended emission, with a flux intensity at least of the same level of that of the central object.

In fig. 4 the same study is shown for the non-Gaussian PSF case. As expected, the reconstructed $\sigma_{\rm src}$ is limited by the tails of the PSF ($\sigma_{\rm PSFtails} = 0.2\,$deg) which represent the minimum size one can aim to reconstruct. As a consequence, a proper reconstruction of the source morphology is not achievable, even for very faint halos. Moreover, when the flux strength of the halo is $\geq 10\%$ of the central source flux, $\sigma_{\rm src}$ is further overestimated: the more extended the halo, the more significant the overestimation of $\sigma_{\rm src}$, since

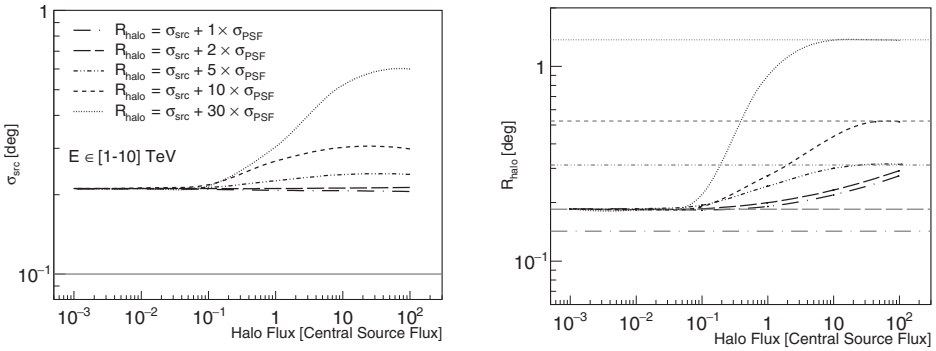

Fig. 4. – Same as in fig. 3 but in the case of a non-Gaussian PSF with tails defined by eq. (5) and calculated for $K = 0.3$. Note that the simulated size of the tails is $\sigma_{\rm PSFtails} = 0.2\,$deg.

the bright emission from the halo adds to the fake emission from the tails and to the central source emission itself. Similarly, in case of weak halos the estimated radius is a constant value ($\sim \sigma_{\rm PSFtails}$). The only way to ensure a proper reconstruction of the halo morphology in case of tails in the PSF is to look at extended objects ($R_{\rm halo} > \sigma_{\rm PSFtails}$) brighter than the central compact source.

5. – Conclusions

Making use of the publicly available performance of a possible layout for the CTA southern observatory, the basic features of this next-generation IACT array have been parameterized and used to characterize a generic CTA-like observatory. The potential of the instrument to perform morphological studies has been investigated. In addition to the ideal Gaussian shaped PSF, more realistic non-Gaussian PSFs with tails have been considered. On the basis of simulations of isolated objects the effect of these tails has been evaluated. The presence of the tails in the PSF creates an additional fake emission, which compromises reliable assessments of the source morphology, since the size of the tails is the minimum size one can aim to reconstruct in case of good instrument sensitivity. The capability of the instrument to disentangle multiple objects clustering in the same region has been found to be significantly reduced due to the additional noise coming from the tails of the PSF. The capability of resolving two nearby sources is limited to the case of sources > 1 degree apart. This study is of particular interest in the contest of gamma-ray emitters located in the complex region of the Galactic plane, where the chance of clustering of two or more gamma-ray sources within 1 degree is high. Moreover, simulations of compact objects on top of diffuse halos, illustrating the case of AGNs surrounded by extended emissions, have been perfomed. The worsening of the instrument potential, due to the presence of the tails in the PSF, further restricts the chance to isolate the two objects, preventing the reconstruction of the diffuse emission in case of moderatly faint (*i.e.* weaker than the central source) and narrow (*i.e.* with a typical size smaller than the size of the tails) halos.

REFERENCES

[1] Horns D. and the HESS Collaboration, *J. Phys.: Conf. Ser.*, **60** (2007) 119.
[2] Firpo R. and the MAGIC Collaboration, *J. Phys.: Conf. Ser.*, **110** (2008) 062009.
[3] Holder J. and the VERITAS Collaboration, in *AIP Conf. Proc.*, **1085** (2009) 657.
[4] Acharya B. S. and the CTA Consortium, *Astrophys. J.*, **43** (2013) 3.
[5] Hassan T. *et al.*, *Second large-scale Monte Carlo study for the Cherenkov Telescope Array*, in *Proceedings of Science* (*ICRC2015*), The Hague, Netherlands.
[6] Ambrogi L., Aharonian F. and De Oña Wilhelmi E., *Astrophys. J.*, **80** (2016) 22.
[7] Bernlohr K. *et al.*, *Astrophys. J.*, **43** (2013) 171.
[8] Aharonian F. *et al.*, *Astron. Astrophys.*, **457** (2006) 899.
[9] Aharonian F. *et al.*, *Astrophys. J.*, **614** (2004) 897.